Chinese Chemical Letters 36 (2025) 110629

Contents lists available at ScienceDirect

Chinese Chemical Letters

journal homepage: www.elsevier.com/locate/cclet

Polymer microparticles with ultralong room-temperature phosphorescence for visual and quantitative detection of oxygen through phosphorescence image and lifetime analysis

Zeyin Chen, Jiaju Shi, Yusheng Zhou, Peng Zhang, Guodong Liang*

PCFM Lab, School of Materials Science and Engineering, Sun Yat-sen University, Guangzhou 510275, China

ARTICLE INFO

Article history:
Received 4 September 2024
Revised 6 November 2024
Accepted 8 November 2024
Available online 9 November 2024

Keywords:
Room-temperature phosphorescence (RTP)
Flexible polymer
Ultralong lifetimes
Doping
Oxygen detection

ABSTRACT

Room-temperature phosphorescence (RTP) materials exhibiting long emission lifetimes have gained increasing attention owing to their potential applications in encryption, anti-counterfeiting, and sensing. However, most polymers exhibit a short RTP lifetime (<1 s) because of their unstable triplet excitons. Herein, a new strategy of polymer chain stabilized phosphorescence (PCSP), which yields a new kind of RTP polymers with an ultralong lifetime and a sensitive oxygen response, has been reported. The rigid polymer chains of poly(methyl mathacrylate) (PMMA) immobilize the emitter molecules through multiple interactions between them, giving rise to efficient RTP. Meanwhile, the loosely-packed amorphous polymer chains allow oxygen to diffuse inside, endowing the doped polymers with oxygen sensitivity. Flexible and transparent polymer films exhibited an impressive ultralong RTP lifetime of 2.57 s at room temperature in vacuum, which was among the best performance of PMMA. Intriguingly, their RTP was rapidly quenched in the presence of oxygen. Furthermore, RTP microparticles with a diameter of 1.63 μm were synthesized using *in situ* dispersion polymerization technique. Finally, oxygen sensors for quick, visual, and quantitative oxygen detection were developed based on the RTP microparticles through phosphorescence lifetime and image analysis. With distinctive advantages such as an ultralong lifetime, oxygen sensitivity, ease of fabrication, and cost-effectiveness, PCSP opens a new avenue to sensitive materials for oxygen detection.

Oxygen detection is of great importance across diverse fields including environmental monitoring, industrial process control, medical diagnostics, and biological sciences [1–4]. In the industrial sector, oxygen detectors ensure the safe and efficient operation of processes requiring precise control of oxygen levels, such as combustion and fermentation. In environmental monitoring, they are used to assess air quality and the health of aquatic ecosystems. In the medical field, oxygen detectors are crucial for monitoring patient blood oxygen saturation, vital for respiratory management and disease diagnosis. Currently, the most commonly used methods for oxygen detection primarily rely on electrochemical techniques which base on the reduction of oxygen at an electrode, generating a measurable electrical signal proportional to the oxygen concentration. However, electrochemical methods are plagued with several inherent limitations, including sluggish response rates, susceptibility to moisture, and compromised sensitivity due to the nonlinear relationship between output signals and oxygen concentration. Consequently, there is an urgent need for the development of rapid and highly sensitive methods for oxygen detection [5–7].

Room-temperature phosphorescence (RTP) materials, exhibiting a long lifetime ranging from milliseconds to seconds, have garnered increasing attention due to their promising applications in sensing, anti-counterfeiting, encryption, and so on [8–15]. However, pure polymers normally fail to exhibit RTP properties under ambient conditions due to the instability of their triplet excitons [16,17]. Recently, a range of RTP polymers have been developed by stabilizing triplet excitons through various strategies, including crystallization, molecular packing, polymerization, host-guest inclusion complexes, and doping [18–26]. Among these preparation methods, doping emitter molecules into polar and crystalline polymer matrices has proven to be a robust approach for the facile fabrication of RTP materials [27–32]. Chromophores are incorporated into polymers through melt or solution mixing or copolymerization, resulting in their immobilization within the polar polymer matrix [33–35]. The strong interaction among the polymer chains and the densely-packed polymer crystals stabilize the excitons and suppress their nonradiative decay pathways, thus yielding brightly

* Corresponding author.
E-mail address: lgdong@mail.sysu.edu.cn (G. Liang).

https://doi.org/10.1016/j.cclet.2024.110629
1001-8417/

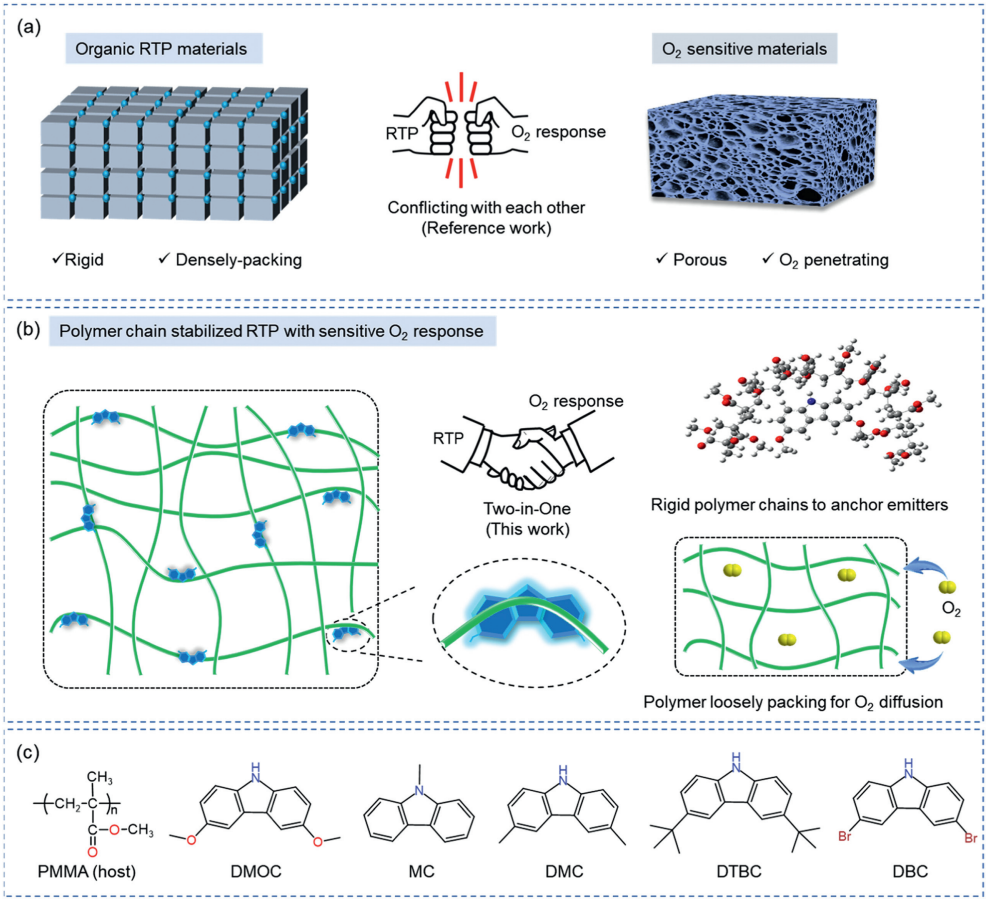

Fig. 1. (a) Schematic illustration of RTP and oxygen-sensitive materials reported in the literature. (b) Schematic illustration of polymer chain stabilized RTP with sensitive oxygen response. (c) Chemical structures of polymer and the emitter molecules used.

luminescent RTP materials [36–43]. Yang and Zhao incorporated aromatic chromophores into polymer matrices, creating RTP materials that exhibit multiple stimulus-responses [44–47]. Li and Zhang doped acriflavine into polyvinyl alcohol (PVA) and obtained visible-light-excited fluorescence afterglow with a quantum yield of 42.4% [48]. Tang and Xiong prepared UV-responsive RTP polymers by doping PVA with aromatic emitter compounds [49,50]. In recent years, a variety of RTP polymers have been achieved by doping strategies. Nevertheless, the majority of reported polymeric materials still exhibit RTP lifetimes shorter than 1 s [51–54]. Therefore, the development of RTP polymers with lifetimes exceeding 1 s remains highly desirable for their potential application in sensing.

RTP is highly susceptible to atmospheric oxygen molecules and can be easily quenched by them. This is due to the triplet excitons involving in the photophysical process of RTP, are prone to deactivate through nonradiative pathways in the presence of oxygen. Such an oxygen-responsive behavior of RTP materials offers an alternative approach for oxygen detection [55]. More importantly, RTP exhibits a prolonged lifetime up to seconds, making its lifetime decay readily discernible even with the naked eye. This observable RTP decay offers a compelling opportunity for the visual sensing of oxygen. Furthermore, differing from emission intensity and color, lifetime representing the duration of emission intensity decay serves as a self-referenced parameter, offering an ideal parameter for sensing applications. However, to achieve efficient RTP, polar and crystalline polymers are typically employed as a matrix. The robust interaction among the polymer chains and their dense packing effectively immobilize the chromophore molecules and suppress nonradiative decay pathways. While this strong interaction and dense packing enhance RTP, they also restrict the diffusion of oxygen through the polymeric material, posing a challenge for oxygen sensing (Fig. 1). Therefore, although several long-lived RTP polymers have been reported [56,57], their exploration for oxygen detection remains limited.

Herein, we report a novel approach to stabilize triplet excitons through the utilization of rigid polymer chains. This innovative strategy leads to the creation of a unique type of amorphous RTP polymers that possess an exceptionally long lifetime and oxygen sensitivity. The rigid polymer chains effectively immobilize chromophore molecules through numerous interactions, resulting in efficient RTP. Simultaneously, the loose packing of the amorphous polymer chains allows for oxygen diffusion within, conferring oxygen sensitivity to the doped polymers (Fig. 1). As a demonstration of concept for polymer chain stabilized phosphorescence (PCSP), an engineering plastic of poly(methyl methacrylate) (PMMA) was used as a matrix because of its high glass transition temperature and O_2 gas permeability. And carbazole derivatives were utilized as dopants for their strong interaction with PMMA. These resultant doped amorphous polymer films were flexible and transparent, and exhibited an impressive ultralong lifetime of 2.57 s at room temperature in vacuum, which was one of the best performances of PMMA-based RTP materials. Interestingly, in the presence of oxygen, their RTP turned off quickly through a dynamic collisional mechanism. Furthermore, RTP microparticles with a diameter of 1.63 μm were synthesized using *in situ* dispersion polymerization technique to verify the universality of PCSP. Finally, quick, visual, and quantitative sensing of oxygen was fulfilled through phosphorescence lifetime and image analysis of the RTP microparticles. To

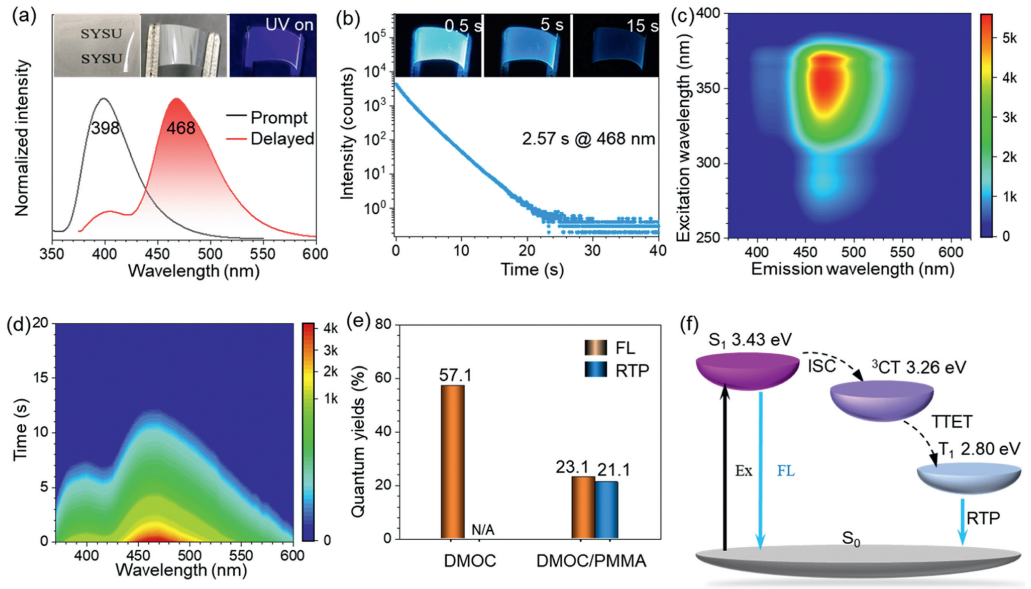

Fig. 2. (a) Fluorescence (black) and phosphorescence (delay 100 ms, red) emission spectra of DMOC/PMMA at room temperature in N_2. Inset showed digital images of the doped polymer films under daylight and UV light. (b) Decay profile of the RTP lifetime of DMOC/PMMA in N_2. Excitation: 365 nm. Inset showed digital images of the doped polymer films after the cease of UV light. (c) Two-dimensional excitation-phosphorescence emission mapping. (d) Transient photoluminescence decay mapping. (e) Fluorescence and RTP quantum yields of DMOC powders and DMOC/PMMA (0.5 wt%) in N_2. (f) Proposed mechanism of RTP of DMOC/PMMA.

the best of our knowledge, this is the first report on ultralong RTP microparticles for oxygen sensing. Given the distinctive advantages, including ultralong lifetime, oxygen sensitivity, ease of fabrication, and cost-effectiveness, PCSP presents a novel platform for creating sensitive materials for oxygen detection.

A carbazole derivative of DMOC was chosen as an emitter, and was doped into PMMA by melt mixing them. The doped polymers of DMOC/PMMA (0.5 wt%) were transparent and flexible, and emitted bright deep blue fluorescence at a wavelength of 398 nm under UV irradiation (365 nm) (Fig. 2a). And the deep blue color immediately turned into blue and faded slowly after ceasing UV excitation. The blue RTP could be observed with the naked eye at room temperature in vacuum. The RTP spectra of DMOC/PMMA showed a distinct peak at 468 nm with an ultralong lifetime of 2.57 s (Fig. 2b). Notably, the RTP spectrum of DMOC/PMMA resembled that of DMOC (Figs. S1–S7 in Supporting information), demonstrating that the RTP of DMOC/PMMA emanated from DMOC. Because neither DMOC nor PMMA emitted RTP, the RTP of DMOC/PMMA was ascribed to the emitter molecules dispersed in PMMA matrix. The emitter molecules were anchored onto rigid polymer chains through strong and abundant interaction between them, which stabilized the triplet excitons and consequently activated their radiative decay pathway, resulting in an ultralong RTP. Excitation-RTP mapping of DMOC/PMMA revealed that its RTP could be excited in a broad wavelength range of 270–390 nm. Nevertheless, its maximum RTP wavelength rarely depended on excitation wavelength (Figs. 2c and d, and Fig. S8 in Supporting information), suggesting homogeneous dispersion of DMOC molecules in PMMA matrix likely due to the strong interaction between them. Intriguingly, DMOC/PMMA exhibited a high RTP quantum yield of 21.1% (Fig. 2e and Fig. S9 in Supporting information), which is highly desirable for its further sensing applications. Therefore, the emitter molecules of the doped polymers are excited to singlet excited states (S_1) under UV light. The energy of S_1 was transferred to ^{3}CT, followed by further transferring to the triplet excited state (T_1) of the emitter molecules. When T_1 returns to the ground state (S_0) through radiative decay pathway, RTP is emitted (Fig. 2f and Fig. S10 in Supporting information). Moreover, the energy levels of singlet and triplet excited states of DMOC/PMMA were theoretically calculated using time-dependent density-functional theory (TD-DFT). The calculated energy levels of singlet and triplet excited states were well consistent with the experimental results (Fig. S11 in Supporting information). For instance, S_1 and T_1 were 3.51 and 2.68 eV respectively, agreeing with the experimental values (3.43 and 2.80 eV, respectively).

DMOC/PMMA polymer films were transparent and flexible, which was favourable for their applications. No emitter aggregates were discerned in the doped film, implying uniform dispersion of emitter molecules in polymer matrix. X-ray diffractometry (XRD) spectra showed that the DMOC crystalline peaks were absent in the XRD spectra of DMOC/PMMA (Fig. 3a), verifying that DMOC molecules were uniformly dispersed in PMMA matrix. UV–vis spectra of DMOC/PMMA showed an absorbance band at 312 nm, which red-shifted compared to that of emitter (Fig. 3b). Moreover, FT-IR spectra of DMOC/PMMA showed an absorbance band at 1578 cm^{-1} (Fig. 3c), which was ascribed to bending vibration of N–H and blue-shifted compared to that of DMOC (1576 cm^{-1}). Such absorbance shifts revealed the strong interaction between the emitter molecules and polymer chains. Moreover, electrostatic potential for DMOC and PMMA was analyzed using the wave function analysis program Multiwfn and the visualization program VMD. It is evident that oxygen atoms in PMMA present dense electron clouds with an electrostatic potential of −37.31 kcal/mol, which act as hydrogen-bonding donors. While the hydrogen atoms in amine moiety of DMOC show fewer electron clouds with an electrostatic potential of +44.58 kcal/mol, serving as hydrogen-bonding acceptors (Fig. 3d and Fig. S12 in Supporting information). Thus, hydrogen-bonding forms in DMOC/PMMA. To investigate the conformational arrangement of DMOC molecules within the PMMA matrix, we employed a combined quantum mechanics and molecular mechanics (QM/MM) simulations for the DMOC/PMMA system using the Gaussian software (Figs. 3e and f, and Fig. S13 in Supporting information). Our findings revealed that the distances between DMOC molecules and their adjacent PMMA chains ranged from 2.16 Å to 3.36 Å. Notably, a diverse array of interaction forces were observed between DMOC and PMMA chains, including N–H···O, C–H···O, C–H···N, and π-H···O interactions. Notably, the preponderance of short-range N–H···O (2.16 Å) and π-H···O (2.69 Å)

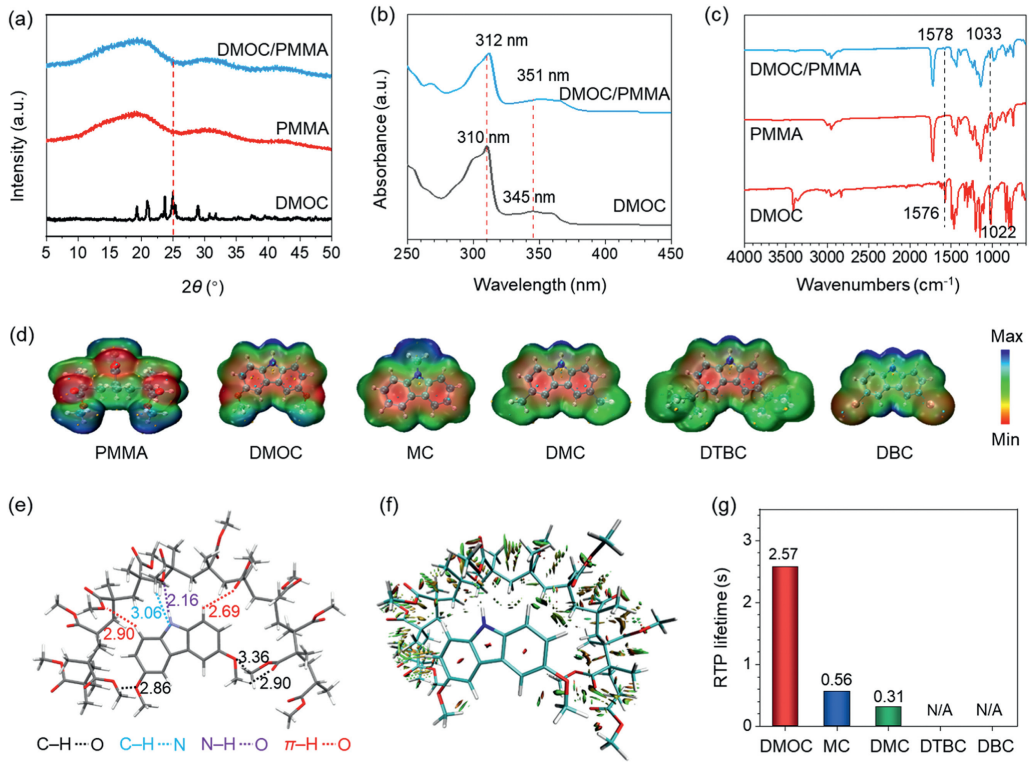

Fig. 3. (a) XRD spectra of DMOC, PMMA, and DMOC/PMMA. (b) UV–vis spectra of DMOC and DMOC/PMMA. (c) FT-IR spectra of DMOC, PMMA, and DMOC/PMMA. (d) Electrostatic potential analysis of chromophores and PMMA. (e) Interaction between DMOC and PMMA. (f) Reduced density gradient (RDG) isosurface mapping of DMOC molecules in PMMA with an isovalue of 0.5. (g) RTP lifetime of PMMA doped with various emitters.

interactions significantly immobilized the DMOC molecules. These results suggest that the PMMA chains offer a rigid and strongly interactive environment for DMOC, thereby playing a pivotal role in suppressing the nonradiative decay of triplet excitons.

The effect of dopants on RTP was investigated. A series of analogs of emitter molecules with similar chemical structures, including MC, DMC, DTBC, and DBC, were used to dope PMMA for comparison (Fig. 3g and Figs. S14–S16 in Supporting information). Among the doped materials, DMOC/PMMA showed the maximum RTP lifetime and efficiency, likely due to the high polarity of DMOC enhancing its interaction with the polymer matrix.

Intriguingly, the RTP properties of DMOC/PMMA exhibited a dependency on UV radiation duration (Fig. S17 in Supporting information). Initially, the as-prepared polymer film displayed weak RTP. However, as the UV radiation duration was extended to 12 s, both the RTP intensity and lifetime underwent a remarkable surge. Thereafter, the RTP intensity and lifetime reached a stable plateau. Notably, the RTP characteristics of the doped polymer film were particularly sensitive to oxygen exposure. Exposure of the film to air for just 1 min resulted in RTP quenching of the doped polymer film. This phenomenon holds significant promise for oxygen detection applications. The residual oxygen present in the as-prepared film deactivates the triplet excitons, leading to the observed weak RTP. Prolonging the UV radiation duration effectively consumes the oxygen within the doped film. This allows the triplet excitons to return to the ground state through a radiative decay pathway, thereby enhancing the RTP and resulting in UV-triggered RTP. When the RTP polymer film is subsequently exposed to oxygen, the oxygen molecules diffuse through the film and quench the RTP. Consequently, UV-activated and oxygen-sensitive RTP is achieved.

DMOC/PMMA materials could be *in situ* synthesized by using dispersion polymerization technique, allowing the fabrication of monodispersed microparticles of the RTP materials. Scanning electron microscopy (SEM) images showed that spherical particles with a diameter of 1.63 ± 0.47 μm formed after dispersion polymerization (Figs. 4a–c). Phosphorescence spectra showed that the microparticles exhibited similar RTP emission with the bulk materials (Fig. S18 in Supporting information). RTP lifetime decay profile revealed that the microparticles showed a slightly decreased lifetime compared to the bulk materials (2.17 s and 2.57 s, respectively, due to high mobility of polymer chains at the surface of particles, consistent with the previous reports [58]. The microparticles inherited the oxygen sensitivity from the bulk materials. The microparticles did not show RTP in air. While upon purging with nitrogen gas, the RTP of the N_2-purged area boosted. Exposure of the N_2-purged microparticle films in air for 1 min, their RTP disappeared again. Such oxygen-sensitive RTP property is highly valuable for oxygen detection in air.

Encouraged by the remarkable oxygen sensitivity, we developed oxygen sensors utilizing the RTP microparticles. Employing a technique based on phosphorescence lifetime and image analysis (PLIA), we achieved rapid, visual, and quantitative oxygen sensing. The RTP microparticles films were exposed to oxygen/nitrogen mixed gas and excited using a UV flashlight at 365 nm (Fig. 4d). Videos were recorded using a commercial mobile phone camera. Video screenshots at various times were analyzed (Fig. S19 in Supporting information). The blue values of RTP images were calculated using a Matlab program. The plot of blue values versus time for each oxygen fraction was obtained. The blue values decreased exponentially against time (Fig. 4e, Figs. S20–S27, and Table S1 in Supporting information). The RTP lifetime was obtained by data fitting. Intriguingly, the ratio of τ_0/τ exhibited a linear correlation with the oxygen fraction, revealing a dynamic collisional quenching mechanism of RTP by oxygen (Fig. 4f). To demonstrate the practical applications of our oxygen sensors, we exposed the RTP microparticle films to air with an oxygen fraction of 0.5%. The RTP lifetime

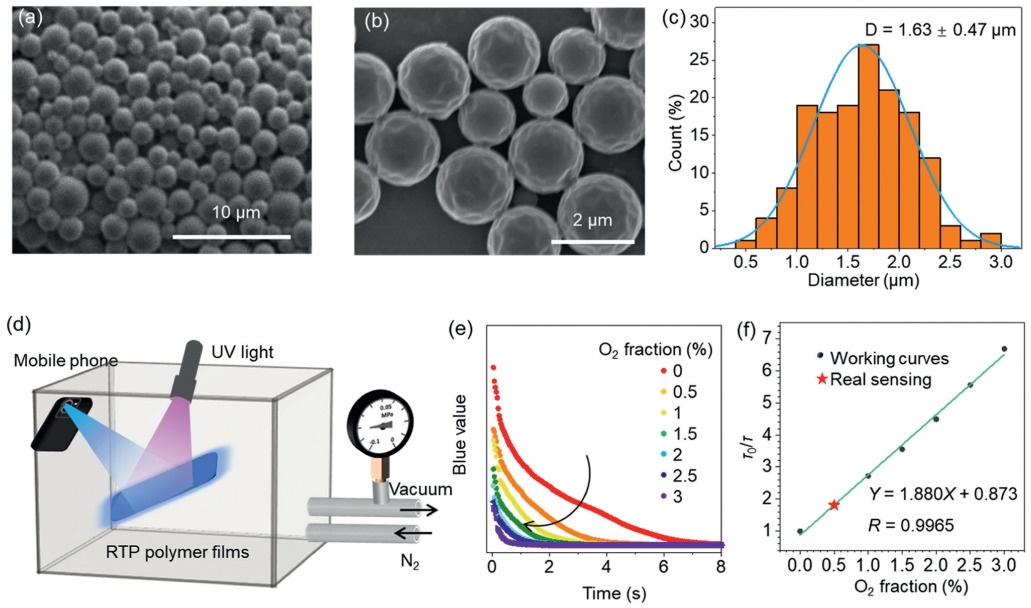

Fig. 4. (a, b) Scanning electron microscopy (SEM) images of DMOC/PMMA microparticles. (c) Diameter distribution of DMOC/PMMA microparticles. (d) Schematic illustration of oxygen detection using the ultralong RTP polymer microparticles films. (e) Blue values of RTP images as function of delay time. (f) The plot of τ_0/τ (τ_0 and τ are RTP lifetime in the absent and presence of oxygen, respectively).

was measured to be 1.331 ± 0.066 s by PLIA. Using the established working curve, we calculated the oxygen fraction to be 0.499% ± 0.050%, achieving a satisfactory recovery of 99.8% (Fig. 4f, Fig. S28, and Table S2 in Supporting information). These results demonstrate the potential of our oxygen sensors based on ultralong RTP polymers for real-world applications. Finally, reproducibility of oxygen sensors was checked by repeatedly switching between in vacuum and air. Similar blue values and lifetimes were obtained with increasing cycle numbers (Figs. S29 and S30 in Supporting information), demonstrate the superb reproducibility of the oxygen sensors. Our oxygen sensors based on ultralong RTP polymers possesses overwhelming advantages: (1) Self-referenced. No calibration is required because self-referenced parameter of lifetime is used. (2) Simple instruments. Taking advantage of ultralong RTP lifetimes over 2 s, RTP images can be readily captured with a common smartphone camera. RTP lifetimes can be determined through PLIA technique, which are independent of imaging equipment, uneven color distribution, and possible color discrepancies caused by background, containers, or light scattering. (3) Simple data analysis. RTP lifetime, depicting decay of RTP intensity, is independent of RTP color or CIE coordinates. Thus, there is no need to determine accurately RTP CIE coordinates. Our oxygen sensors are based on blue RTP (468 nm), and blue value is valid enough to determine RTP lifetime.

In summary, a novel strategy of polymer chain stabilized phosphorescence (PCSP) has been reported, yielding a new family of RTP polymers that exhibit an exceptionally long lifetime and a highly sensitive response to oxygen. The polymer chains effectively immobilize chromophore molecules through multiple interactions, promoting efficient RTP. Simultaneously, the amorphous polymer chains are loosely packed, facilitating oxygen diffusion within them, thereby conferring oxygen sensitivity to the doped polymers. These flexible and transparent polymer films exhibit an ultralong RTP lifetime of 2.57 s coupled with a high efficiency of 21.1% at room temperature in vacuum. Notably, their RTP is rapidly quenched in the presence of oxygen through a dynamic collisional quenching mechanism. Furthermore, RTP microparticles with a diameter of 1.63 μm are synthesized using *in situ* dispersion polymerization technique. Finally, phosphorescence lifetime and image analysis of the RTP microparticles enables rapid, visual, and quantitative oxygen sensing. With its unique advantages, including an ultralong lifetime, oxygen sensitivity, ease of fabrication, and cost-effectiveness, PCSP offers a novel avenue for the development of sensitive materials for oxygen detection.

Declaration of competing interest

The authors declare that they have no known competing financial interests or personal relationships that could have appeared to influence the work reported in this paper.

CRediT authorship contribution statement

Zeyin Chen: Writing – original draft, Formal analysis, Data curation. **Jiaju Shi:** Data curation. **Yusheng Zhou:** Data curation. **Peng Zhang:** Supervision, Formal analysis. **Guodong Liang:** Writing – review & editing, Supervision, Project administration, Funding acquisition.

Acknowledgments

The financial support is partially from National Natural Science Foundation of China (No. 22475241), Guangdong Basic and Applied Basic Research Foundation (Nos. 2022A1515010826 and 2023A1515012696) and the Fundamental Research Funds for the Central Universities (Nos. 17lgjc03 and 18lgpy04).

Supplementary materials

Supplementary material associated with this article can be found, in the online version, at doi:10.1016/j.cclet.2024.110629.

References

[1] J.Z. Zhao, W.H. Wu, J.F. Sun, S. Guo, Chem. Soc. Rev. 42 (2013) 5323–5351.
[2] X.D. Wang, O.S. Wolfbeis, Chem. Soc. Rev. 43 (2014) 3666–3761.
[3] Y.C. Yu, M.S. Kwon, J. Jung, et al., Angew. Chem. Int. Ed. 56 (2017) 16207–16211.
[4] Y. Zhou, W. Qin, C. Du, et al., Angew. Chem. Int. Ed. 58 (2019) 12102–12106.
[5] R.Y. Xu, Y.F. Wang, X.P. Duan, et al., J. Am. Chem. Soc. 138 (2016) 2158–2161.

[6] E. Roussakis, Z.X. Li, A.J. Nichols, C.L. Evans, Angew. Chem. Int. Ed. 54 (2015) 8340–8362.
[7] S.Y. Liu, D.D. Zhou, C.T. He, et al., Angew. Chem. Int. Ed. 55 (2016) 16021–16025.
[8] J. Yang, M.M. Fang, Z. Li, Acc. Mater. Res. 2 (2021) 644–654.
[9] H. Gao, X. Ma, Aggregate 2 (2021) e38.
[10] B.B. Ding, X. Ma, H. Tian, Acc. Mater. Res. 4 (2023) 827–838.
[11] W.B. Dai, Y.T. Jiang, Y.X. Lei, et al., Chem. Sci. 15 (2024) 4222–4237.
[12] Z.J. Song, Y. Shang, Q. Lou, et al., Adv. Mater. 35 (2023) 2207970.
[13] Q. Lou, N. Chen, J.Y. Zhu, et al., Adv. Mater. 35 (2023) 2211858.
[14] A.R. Huang, Y.Y. Fan, K. Wang, et al., Adv. Mater. 35 (2023) 2209166.
[15] M.X. Gao, Y. Tian, X.N. Li, et al., Angew. Chem. Int. Ed. 62 (2022) e202214908.
[16] J.Y. Zhou, D.P. Liu, L.Q. Li, et al., Chin. Chem. Lett. 35 (2024) 109929.
[17] T.T. Wang, M. Liu, J.Y. Mao, et al., Chin. Chem. Lett. 35 (2024) 108385.
[18] Y.F. Zhang, C.C. Xiong, W.B. Wang, et al., Aggregate 4 (2023) e310.
[19] Y. Zhang, W. Zhang, J. Xia, et al., Angew. Chem. Int. Ed. 62 (2023) e202314273.
[20] W. Qin, J. Ma, Y.S. Zhou, et al., Chem. Eng. J. 400 (2020) 125934.
[21] J. Ma, Y.S. Zhou, H.Y. Gao, et al., Mater. Chem. Front. 5 (2021) 2261–2270.
[22] Y.J. Yang, J.Q. Wang, J. Yang, et al., Angew. Chem. Int. Ed. 62 (2023) e202218994.
[23] X.X. Liu, Q.Y. Liao, J. Yang, et al., Angew. Chem. Int. Ed. 62 (2023) e202302792.
[24] T.W. Zhu, T.J. Yang, Q. Zhang, W.Z. Yuan, Nat. Commun. 13 (2022) 2658.
[25] S.X. Tang, Z.H. Zhao, J.Q. Chen, et al., Angew. Chem. Int. Ed. 61 (2022) e202117368.
[26] X.Y. Dou, T.W. Zhu, Z.S. Wang, et al., Adv. Mater. 32 (2020) 2004768.
[27] X.P. Wang, J.B. Li, Y. Zeng, et al., Chem. Eng. J. 460 (2023) 141916.
[28] G.M. Wang, J.Y. Li, X. Li, et al., Chem. Eng. J. 431 (2022) 134197.
[29] G.M. Wang, X.F. Chen, X. Li, et al., Chem. Sci. 14 (2023) 8180–8186.
[30] X.H. Zhang, K.C. Chong, Z.L. Xie, B. Liu, Angew. Chem. Int. Ed. 62 (2023) e202310335.
[31] K.C. Chong, C.J. Chen, C. Zhou, et al., Adv. Mater. 34 (2022) 2201569.
[32] C.J. Chen, Z.G. Chi, K.C. Chong, et al., Nat. Mater. 20 (2021) 175–180.
[33] T. Zhang, X. Ma, H.W. Wu, et al., Angew. Chem. Int. Ed. 59 (2020) 11206–11216.
[34] X.Y. Yao, J. Wang, D.J. Jiao, et al., Adv. Mater. 55 (2020) 2005973.
[35] Z.A. Yan, X.H. Lin, S.Y. Sun, et al., Angew. Chem. Int. Ed. 60 (2021) 19735–19739.
[36] K.J. Chen, Y.F. Zhang, Y.X. Lei, et al., Nat. Commun. 15 (2024) 1269.
[37] Y.H. Liang, C. Xu, H.Q. Zhang, et al., Angew. Chem. Int. Ed. 62 (2023) e202217616.
[38] Y.H. Liang, P.T. Hu, H.Q. Zhang, et al., Angew. Chem. Int. Ed. 63 (2024) e202318516.
[39] M.Y. Jian, Z.C. Song, X.J. Chen, et al., Chem. Eng. J. 429 (2022) 132346.
[40] C. Qian, Z.M. Ma, X.H. Fu, et al., Adv. Mater. 34 (2022) 2200544.
[41] H. Peng, G.Z. Xie, Y. Cao, et al., Sci. Adv. 8 (2022) eabk2925.
[42] H. Li, J. Gu, Z.J. Wang, et al., Nat. Commun. 13 (2022) 429.
[43] X. Yan, H. Peng, Y. Xiang, et al., Small 18 (2022) 202104073.
[44] Z.H. Wang, L. Gao, Y. Zheng, et al., Angew. Chem. Int. Ed. 61 (2022) e202203254.
[45] C. Wang, L.J. Qu, X.H. Chen, et al., Adv. Mater. 34 (2022) 2204415.
[46] Y. Su, Y.F. Zhang, Z.H. Wang, et al., Angew. Chem. Int. Ed. 59 (2020) 9967–9971.
[47] J.J. Guo, C.L. Yang, Y.L. Zhao, Acc. Chem. Res. 55 (2022) 1160–1170.
[48] J.Q. Wang, Y.J. Yang, K.X. Li, et al., Angew. Chem. Int. Ed. 62 (2023) e202304020.
[49] S.D. Xiong, Y. Xiong, D.L. Wang, et al., Adv. Mater. 35 (2023) 2301874.
[50] K.Y. Chen, Y. Xiong, D.L. Wang, et al., Adv. Funct. Mater. 34 (2023) 2312883.
[51] Y.S. Zhou, P. Zhang, Z. Liu, et al., Adv. Mater. 36 (2024) 202312439.
[52] Y.S. Zhou, L.M. Jin, J.Q. Chen, et al., Chem. Eng. J. 463 (2023) 142506.
[53] J.J. Shi, W.J. Tao, Y.S. Zhou, G.D. Liang, Chem. Eng. J. 475 (2023) 146178.
[54] W.J. Tao, Y.S. Zhou, F.X. Lin, et al., Adv. Opt. Mater. 10 (2022) 202102449.
[55] L. Zhang, F. Gu, P. Jiang, X. Ma, ACS Appl. Mater. Inter. 16 (2024) 42794–42801.
[56] Y.Y. Zhao, J.H. Yang, C. Liang, et al., Angew. Chem. Int. Ed. 63 (2023) e202317431.
[57] X. Zou, N. Gan, M.Y. Dong, et al., Adv. Mater. 35 (2023) 202210489.
[58] J.J. Shi, Y.S. Zhou, W. Wang, et al., Chem. Eng. J. 492 (2024) 152419.